Neurobiology of Disease 124 (2019) 1–13

Contents lists available at ScienceDirect

Neurobiology of Disease

journal homepage: www.elsevier.com/locate/ynbdi

Phenotypic and molecular features underlying neurodegeneration of motor neurons derived from spinal and bulbar muscular atrophy patients

Marianne Sheila[a,b,*,1,2], Gunaseelan Narayanan[a,3,2], Siming Ma[c], Wai Leong Tam[c], Josiah Chai[d], Lawrence W. Stanton[a,*,4]

[a] Stem Cell and Regenerative Biology, Genome Institute of Singapore, Singapore 138672, Singapore
[b] Yong Loo Lin School of Medicine, National University of Singapore, Singapore 119228, Singapore
[c] Cancer Therapeutics and Stratified Oncology, Genome Institute of Singapore, Singapore 138672, Singapore
[d] Department of Neurology, National Neuroscience Institute, Singapore 308433, Singapore

ABSTRACT

Spinal and bulbar muscular atrophy (SBMA) is a neurodegenerative disease caused by the expansion of polyglutamine region in the androgen receptor. To gain insights into mechanisms of SBMA, four wild-type and five SBMA iPSC lines were differentiated to spinal motor neurons (sMNs) with high efficiency. SBMA sMNs showed neurite defects, reduced sMN survival and decreased protein synthesis levels. Microarray analysis revealed a dysregulation in various neuronal-related signalling pathways in SBMA sMNs. Strikingly, *FAM135B* a novel gene of unknown function, was found drastically downregulated in SBMA sMNs. Knockdown of *FAM135B* in wild-type sMNs reduced their survival and contributed to neurite defects, similar to SBMA sMNs, suggesting a functional role of *FAM135B* in SBMA. The degenerative phenotypes and dysregulated genes revealed could be potential therapeutic targets for SBMA.

1. Introduction

Spinal and bulbar muscular atrophy (SBMA) is a neuromuscular disorder characterized by the degeneration of lower motor neurons in males and SBMA patients often experience progressive weakness in the limb and bulbar muscles (Katsuno et al., 2010). SBMA is caused by the abnormal expansion of the CAG repeat region in the first exon of the *Androgen Receptor (AR)* gene on the X-chromosome. Healthy individuals typically have 9 to 36 CAG repeats while SBMA patients have more than 38 CAG repeats (La Spada et al., 1991).

The disease mechanisms underlying SBMA is not fully understood. Previous studies have suggested that the mutant AR may affect several cellular processes including mitochondrial function (Ranganathan et al., 2008), axonal transport (Katsuno et al., 2006), autophagic flux (Cortes et al., 2014) and transcriptional regulation (Lieberman et al., 2002; Suzuki et al., 2009). SBMA pathogenesis has been investigated using model systems such as immortalised cell lines, fly and mouse models (Beitel et al., 2013). SBMA induced pluripotent stem cells (iPSCs) offer an alternative system with a human context for investigating the SBMA pathogenesis. Two previous studies have reported the generation of SBMA iPSC lines (Grunseich et al., 2014; Nihei et al., 2013). Recently, our group has generated iPSCs from two SBMA patients and their healthy siblings (Narayanan et al., 2017).

In this study, we report the differentiation of wild-type (WT) and SBMA iPSC lines to spinal motor neurons (sMNs). Through phenotypic assays and microarray gene expression profiling of the WT and SBMA sMNs, we reveal dysregulated signalling pathways and importantly, highlight a gene of unknown function, *FAM135B,* which could play pathogenic roles in SBMA.

2. Results

2.1. Differentiation of iPSCs to sMNs

To better understand the SBMA disease mechanism, we differentiated patient -derived iPSCs into sMNs. We previously generated iPSC lines using peripheral blood mononuclear cells from two SBMA patients, their healthy siblings and a non-related healthy individual (Narayanan et al., 2017). In addition to these lines, one WT and three SBMA iPSC lines were kindly gifted by the Boehm and Fishbeck laboratories respectively. Hence a total of four WT and five SBMA iPSC lines were used in this study (Table 1). We differentiated the four WT

* Corresponding authors at: Stem Cell and Regenerative Biology, Genome Institute of Singapore, Singapore 138672, Singapore.
E-mail addresses: marianne_sheila@bti.a-star.edu.sg, mariannes99@gis.a-star.edu.sg (M. Sheila), stantonl@gis.a-star.edu.sg (L.W. Stanton).
[1] Present address: Bioprocessing Technology Institute, Singapore 138668, Singapore
[2] **Co-first author.**
[3] Present address: Singapore Stem Cell Bank, Institute of Medical Biology, Singapore 138665.
[4] Present address: Humacyte Inc, Durham, NC 27713, USA.

https://doi.org/10.1016/j.nbd.2018.10.019
Received 8 July 2018; Received in revised form 11 October 2018; Accepted 28 October 2018
Available online 01 November 2018
0969-9961/

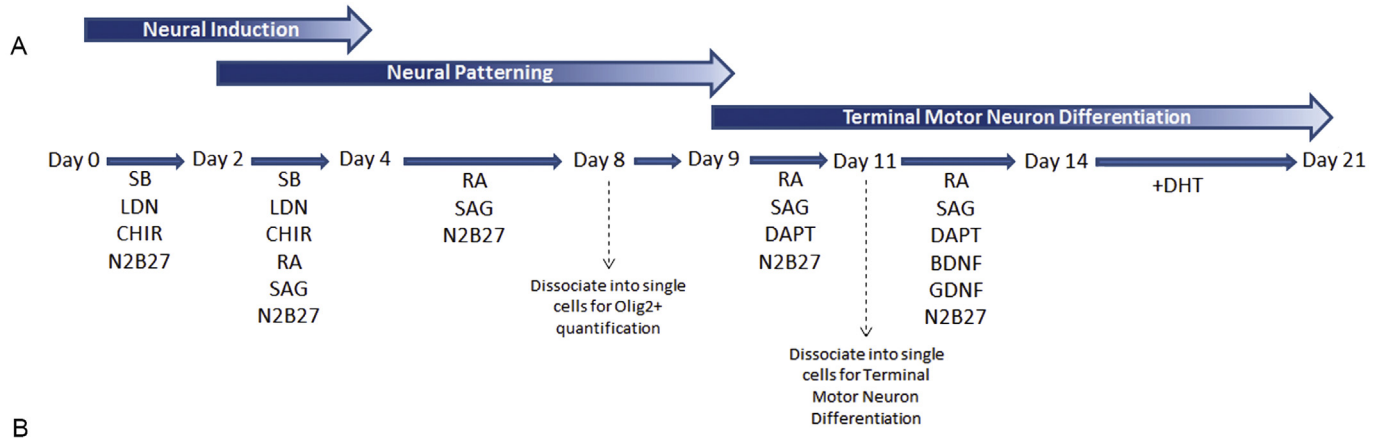

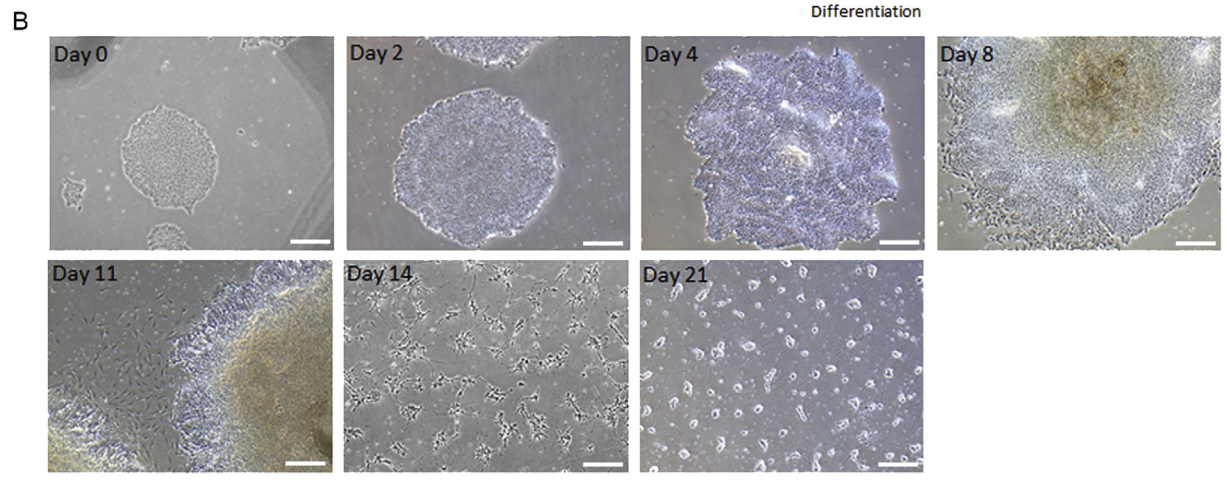

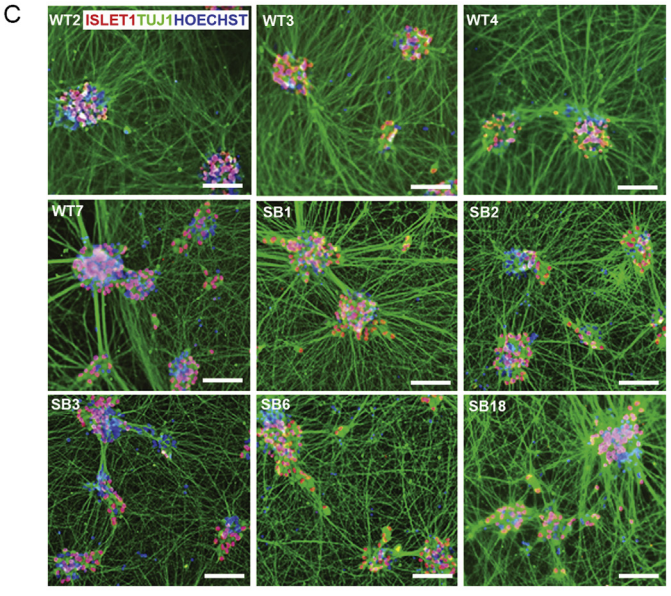

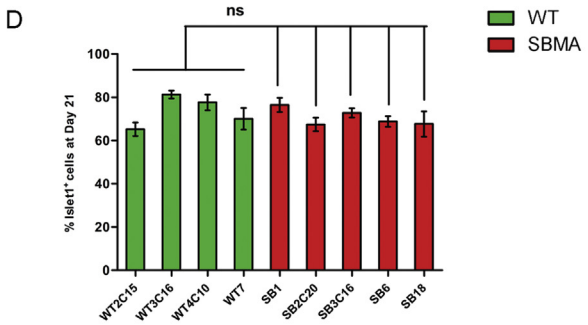

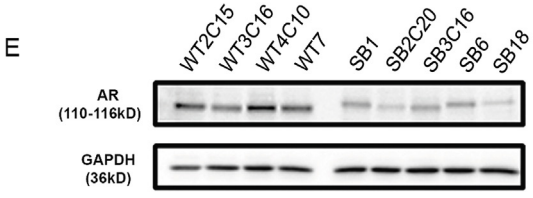

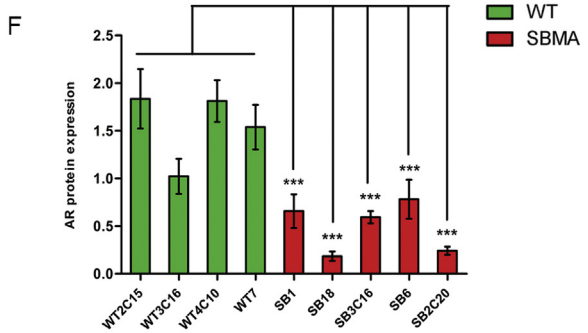

(caption on next page)

Fig. 1. Differentiation of iPSCs to sMNs.
(A) Schematic diagram detailing the sMN differentiation protocol.
(B) Brightfield images illustrating the different stages of sMN differentiation. Scale bar, 50 μm. See also Fig. S1.
(C) Representative immunofluorescence images illustrating that day 21 sMNs express ISLET1 and TUJ1. Scale bar, 100 μm. See also Fig. S1.
(D) Efficiency of sMN generation at day 21 determined by normalizing the number of ISLET1$^+$ sMNs to TUJ1$^+$ cells. Data represent mean ± SEM ($n = 6$), where n refers to the number of independent rounds of sMN differentiation. Comparisons are done by one-way ANOVA followed by Dunnett's test. ns - not significant. See also Fig. S1C.
(E) Representative western blot image showing the expression of AR protein in WT and SBMA day 21 sMNs. See also Fig. S2.
(F) Densitometric quantification of western blot image in (E). Values are normalized to housekeeping protein GAPDH. Data represent mean ± SD ($n = 3$), where n refers to the number of independent rounds of sMN differentiation. Comparisons are done by one-way ANOVA followed by Dunnett's test. ***$p < .001$.

and five SBMA iPSC lines into sMNs using a protocol described previously (Maury et al., 2015) with modifications (Fig. 1A). iPSCs were first induced towards the neural lineage by dual-SMAD inhibition using small molecule inhibitors of TGF-beta signalling (SB-431542) and BMP signalling (LDN-193189) (Chambers et al., 2009), wherein, tightly packed iPSC colonies acquired small gaps between each cell in the colony indicating that they had undergone differentiation (Fig. 1B, day 0 - day 8 and Fig. S1A). A spike of WNT agonist (CHIR-99021) together with RA and SAG, specified neural progenitors to spinal motor neuron progenitors (sMNPs). On day 10, OLIG2$^+$ sMNPs were efficiently (90–95%) generated (Fig. S1B and Fig. S1C). Addition of γ-secretase inhibitor DAPT on day 9 (ie. one day before the highest expression of OLIG2) resulted in rapid specification of post-mitotic sMNs. Two days post DAPT exposure, short neurites extended from edges of the sMNP colonies indicating birth of post-mitotic neurons (Fig. 1B, day 11 and Fig. S1D). By day 14, the post-mitotic neurons arranged themselves in clusters and simple neurite extensions branched out from individual neuronal cell bodies (Fig. 1B, day 14 and Fig. S1E). Several cell and animal models of SBMA have suggested that ligand binding is a key step in SBMA pathogenesis (Katsuno et al., 2002; Takeyama et al., 2002). To better understand the effect of ligand binding on disease outcome, for some studies the AR agonist dihydrotestosterone (DHT) was added from day 14 onwards. By day 21, more complex neurite extensions were seen connecting one neuron cluster to another (Fig. 1B, day 21 and Fig. S1F). At day 21, post-mitotic neurons stained positive for MN markers ISLET1 and CHAT, and pan-neuronal marker TUJ1 (Fig. 1C and Fig. S1G). Quantification of ISLET1$^+$ cells indicated that the efficiency of sMN generation ranged between 65.2% to 81.2% for all nine iPSC lines (Fig. 1D). There was neither a significant difference in the sMN efficiency between the WT or SBMA sMNs (Fig. 1D) nor that in the presence or absence of DHT (Fig. S1H). Western blotting showed that sMNs from all five SBMA lines expressed lower amounts of AR protein as compared to sMNs from all four WT lines at day 21 (Fig. 1E and Fig. 1F). For each line with the exception of SB18, sMNs had higher AR expression when cultured in the presence of DHT than in its absence (Fig. S2A and S2B). No AR aggregates were detected in the SBMA sMNs even when cultured till day 41 (Fig. S2C). These results established that we can efficiently generate sMNs from both healthy donors and SBMA patients who carry the causative mutation of this neurodegenerative disease.

2.2. SBMA sMNs exhibit defects in neurite length and morphology

SBMA patients suffer from degeneration of sMNs. We explored if SBMA sMNs generated in vitro exhibited signs of neurodegeneration. We specifically studied if SBMA sMNs showed defects in their neurite length and morphology. Immunostaining of TUJ1 was performed at day 21 and 31 to visualize neurites and the increase in average neurite length from day 21 to 31 was determined (Fig. 2A). For each line, we found no significant difference in average neurite length increase from day 21 to 31 when cultured in the presence or absence of DHT (Fig. S3A). We further examined data from sMNs cultured in the presence of DHT since DHT is a key player in SBMA pathogenesis. All four WT sMN cultures showed 2.1 to 2.4-fold increases in neurite length from day 21 to 31. However, all five SBMA sMN cultures showed only 1.6 to 1.7-fold increases in neurite length. The increase in neurite length from day 21 to 31 in the SBMA lines was significantly lower than the pooled WT counterpart (Fig. 2B and C) indicating that SBMA sMNs exhibit defects in neurite length compared to WT sMNs.

We also observed morphological differences in the neurites between SBMA and WT sMNs as indicated by punctate staining of TUJ1 along neurites of SBMA sMNs (Fig. 2D). Quantification of this neurite blebbing indicated that at day 21, all SBMA sMN cultures had significantly more blebs per unit neurite length ($p < .001$) than the pooled WT counterpart (Fig. 2E). Increased neurite blebbing is likely indicative of degenerating sMNs.

2.3. SBMA sMNs show reduced survival in prolonged culture

The loss of sMNs is one of the hallmarks of SBMA. We sought to determine if the SBMA sMNs exhibited reduced survival in vitro. Immunostaining of ISLET1 and TUJ1 was performed at day 21 and 41 to visualize the number of sMNs in culture over time (Fig. 3A). For each WT culture, we observed similar number of ISLET1$^+$ sMNs at day 21 and 41. Strikingly, for each of the SBMA cultures, we observed a significant reduction in the number of ISLET1$^+$ sMNs at day 41 compared to day 21 (Fig. 3B). To confirm these observations, we quantified the percentage of day 21 sMNs that survive at day 41. Our data show that in the WT cultures, almost all sMNs survived from day 21 to 41. On the other hand, in the SBMA cultures, only 64.4% to 71.8% of sMNs survived from day 21 to 41. sMNs from all five SBMA cultures showed a significant reduction ($p < .001$) in survival compared to the pooled WT counterpart (Fig. 3C). We determined cleaved caspase-3 levels in day 41 sMNs by Western blotting and found that it was significantly higher in SBMA sMNs, hence validating the decreased survival of SBMA sMNs (Fig. 3D and E). Additionally for each line, we found no significant difference in percentage of day 21 sMNs that survive at day 41 when cultured in the presence or absence of DHT (Fig. S3B).

2.4. SBMA sMNs show defects in protein translation

Previous studies have shown that in neurodegenerative diseases such as Amyotrophic Lateral Sclerosis (ALS), Alzheimer's, Huntington's and Parkinson's disease, protein translation is curbed in response to cellular stress (Hughes and Mallucci, 2018). We therefore checked if protein translation was disrupted in the SBMA sMNs by analyzing the activity of three signalling pathways involved in regulation of protein translation - eIF2α, eIF4/p70S6K and mTOR signalling. We determined the levels of phosphorylated eIF2α, mTOR and p70S6K by Western blotting. Four out of the five SBMA sMNs had significantly higher levels of phosphorylated eIF2α compared to the pooled WT counterpart (Fig. 4A and B). Since phosphorylation of eIF2α leads to down-regulation of protein translation, we measured the level of nascent protein synthesis in WT and SBMA sMNs using a fluorescence-based assay (Click-iT® assay). Data from the assay confirmed that four out of the five SBMA sMNs have significantly reduced protein synthesis compared to the pooled WT counterpart (Fig. 4C).

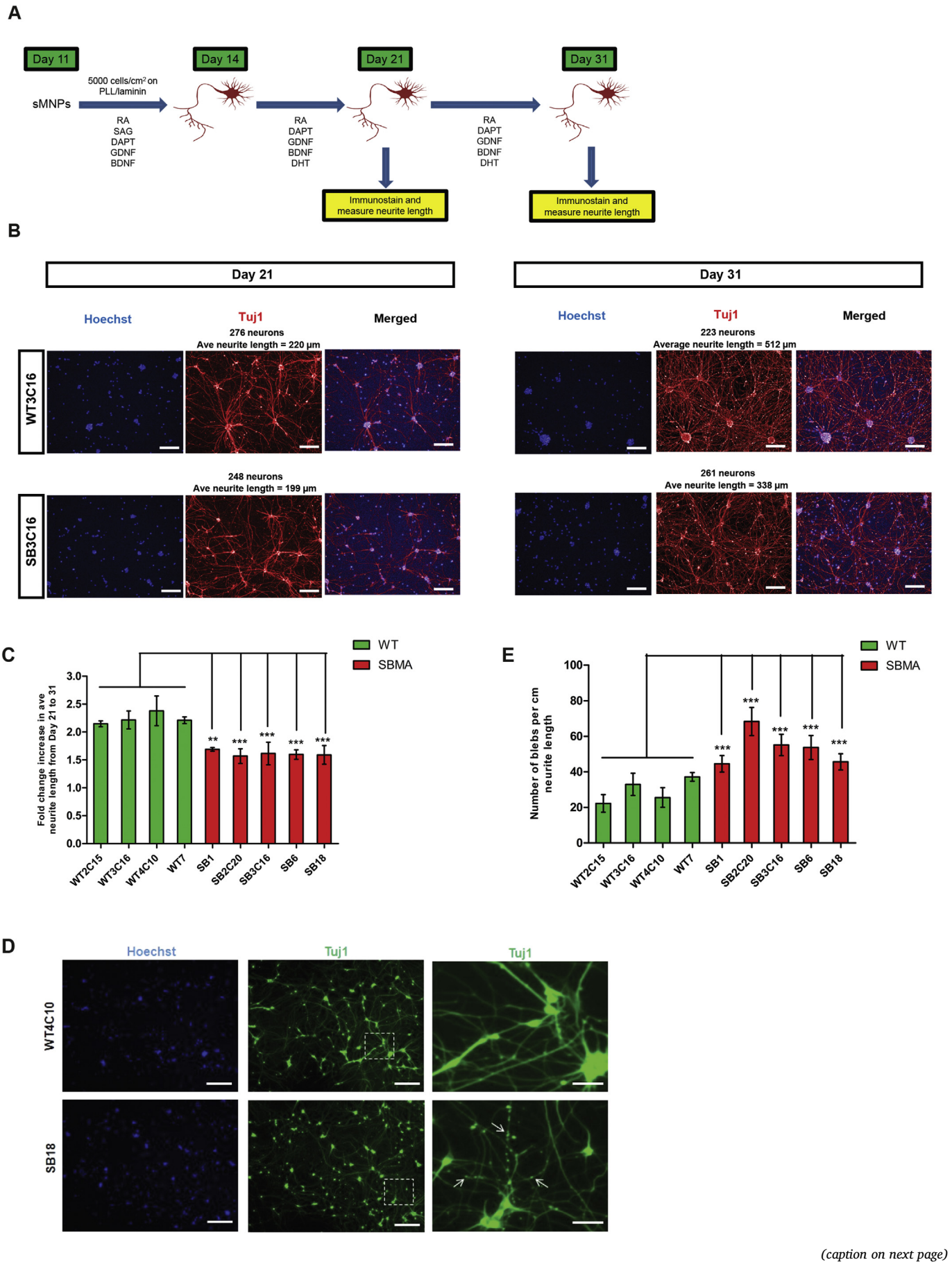

(caption on next page)

Fig. 2. Defects in neurite length of SBMA sMNs.
(A) Schematic representation of neurite length assay.
(B) Representative images of a WT and a SBMA sibling-matched sMN culture stained for TUJ1 at day 21 and 31. SBMA sMNs exhibit reduced neurite outgrowth compared to WT sMNs from day 21 to day 31. Scale bar, 200 μm.
(C) Quantification of neurite length from day 21 to 31. Data represent mean ± SEM (n = 3), where n refers to the number of independent rounds of sMN differentiation. Comparisons are done by one-way ANOVA followed by Dunnett's test. $^{**}p < .01$, $^{***}p < .001$. See also Fig. S3A.
(D) Representative images of a WT and a SBMA sMN culture stained with Hoechst 33342 (leftmost panel) and TUJ1 (middle panel) at day 21. The rightmost panel is a magnified view of the region marked by the white box in the middle panel. White arrows indicate neurite blebs. Scale bar (leftmost and middle panels), 250 μm; scale bar (rightmost panels), 50 μm.
(E) Quantification of neurite blebs per cm neurite length at day 21. Data represent mean ± SEM (n = 3), where n refers to the number of independent rounds of sMN differentiation. Comparisons are done by one-way ANOVA followed by Dunnett's test. $^{***}p < .001$.

2.5. Microarray gene expression profiling implicates novel gene FAM135B

The generation of SBMA sMNs with salient features of neurodegeneration serve as tools to understand the molecular basis of SBMA. We performed microarray gene expression profiling of the WT and SBMA sMNs in the presence and absence of DHT. We first sought to understand the contribution of ligand addition towards disease pathogenesis. Principal Component Analysis (PCA) was applied on the resultant microarray dataset where cell type (SBMA or WT) and treatment type (EtOH or DHT) were included as known covariates. PCA showed that the cell type contributed greater to the clustering of the samples as compared to the treatment type, highlighting the vast transcriptomic disparity that inherently exists between the two disease states and the relatively small disparity between the treatment type (Fig. 5A). Since the disease state contributed greater to the segregation of the samples, we compared the SBMA sMNs to the WT sMNs at either the basal (EtOH) or the DHT condition. Comparison of the SBMA versus the WT sMNs under basal condition (SB.EtOH.vs.WT.EtOH) revealed 405 differentially expressed genes (DEGs) ($p < .05$) while the DHT condition (SB.DHT.vs.WT.DHT) revealed 390 DEG ($p < .05$) (Table S1 and S2). To gain better understanding of all enriched biological processes and biochemical functions, Gene Ontology (GO) analysis was performed using DAVID. Interestingly, GO analysis of downregulated genes in the SB.EtOH.vs.WT.EtOH and SB.DHT.vs.WT.DHT gene lists revealed a top clustering of terms related to neuronal synaptic transmission, neural plasticity and axon development (Fig. 5B and C). This early global downregulation in neuronal-related signalling pathways may contribute to the neurodegenerative phenotypes seen at later time points at both the basal and DHT conditions.

The microarray dataset was then sorted according to FDR *p*-values and fold change differences to reveal the top DEGs in the SB.EtOH.vs.WT.EtOH and SB.DHT.vs.WT.DHT gene lists. Amongst the top 30 genes in the SB.DHT.vs.WT.DHT gene list, 29 (except *ANKRD24*) were also significant in the SB.EtOH. vs. WT.EtOH gene list. Furthermore, these top genes were differentially expressed with the same pattern of dysregulation in both gene lists (Table S3).The substantial overlap in these top DEGs suggests that ligand treatment did not appear to induce an overt effect on the identities of the gene sets in the SBMA sMNs when compared to the WT sMNs. To verify the microarray dataset, the top 10 genes from the SB.DHT.vs.WT.DHT gene list were chosen for further validation via qPCR analysis using sMNs generated from three additional rounds of differentiation. The differential expression of these genes was confirmed by qPCR to be consistent with the microarray expression data (Fig. 5D and Fig. S4A). Of these top ten genes, four genes (*PRPH, FAM135B, DPP6 and ISLR2*) were downregulated and six genes (*ZNF286B, SYNE2, CACNA2D3, SCML1, STXBP6* and *GABRA2*) were upregulated in the SBMA compared to WT sMNs. A number of these genes have been reported to govern important neurobiological processes and alterations in their expression may account for deleterious events affecting SBMA sMNs. Previous studies in various SBMA disease models have implicated the dysregulation in expression levels of cytoskeletal proteins including that of β- tubulin and neurofilament heavy chain protein (Chevalier-Larsen et al., 2004; Yu et al., 2006). In support of these findings, amongst the top ten DEGs, the expression of cytoskeletal-associated proteins *PRPH, SYNE2* and *STXBP6* were found to be dysregulated in the SBMA sMNs. Reduced expression levels of immunoglobulin superfamily protein *ISLR2* and sodium channel modulatory protein *DPP6* have been previously associated with impaired motor neuron axonal projection and survival (Mandai et al., 2009; Sareen et al., 2013). Notably, these genes were downregulated in our SBMA sMNs. Furthermore, presence of electrophysiological abnormalities has been reported in various SBMA models (Juarez-Hernandez et al., 2015; Suzuki et al., 2007). In congruence with these findings, the expression of *CACNA2D3* and *GABRA2,* subunits of important ion channels that govern action potential transmission, were amongst the top ten dysregulated genes. Our study also revealed several novel genes, *FAM135B, SCML1* and *ZNF286B* which have not been previously linked to motor neuron disease.

Following qPCR validation of the microarray data, most strikingly one of the novel genes, *FAM135B*, had a remarkable fold change difference of approximately > 10,000-fold downregulation in a majority of the SBMA sMN lines in comparison to the WT sMN lines (Fig. 5D). Level of *FAM135B* was likewise markedly lower in the SBMA sMNs at the basal condition indicating that the expression of *FAM135B* was not ligand-dependent (Fig. S4B). In healthy brains, the expression of *FAM135B* is apparent within the trigeminal motor nucleus, a region consisting of sMNs that innervate the bulbar muscles (Sunkin et al., 2012; Cruccu et al., 1989). In this regard, the expression of *FAM135B* lends special interest in the context of SBMA as the degeneration of the sMNs and bulbar muscles are hallmarks of SBMA. To validate if this drastic downregulation in *FAM135B* was limited to SBMA, we tested its gene expression levels in iPSC-derived sMNs from ALS and Spinal Muscular Atrophy (SMA) patients. Interestingly, an acute downregulation in *FAM135B* was not apparent in the ALS and SMA disease models indicating that the differential gene expression pattern of *FAM135B* was unique to SBMA (Fig. 5E and F). Intrigued by the drastic downregulation of the largely uncharacterized gene *FAM135B* in the SBMA sMNs and its particular relevance in the context of SBMA, we explored the possible role of *FAM135B* in our disease model.

2.6. Investigating the functional role of FAM135B in SBMA

We investigated if the robust differential expression in *FAM135B* was also apparent at the iPSC stage of the SBMA and WT lines. Interestingly, qPCR analysis showed that *FAM135B* expression was downregulated in all SBMA and WT lines at the iPSC stage and that its differential expression was only observed at the sMN stage (Fig. 6A). The specific downregulation of *FAM135B* in the differentiated cells led us to hypothesize that this gene plays a functional role in supporting sMN growth and survival.

To investigate the potential role of *FAM135B* in the sMNs, we performed a knockdown of *FAM135B* in the WT sMNs and assessed if this downregulation of *FAM135B* affected sMN growth and survival. The neurite length and sMN survival phenotypic assays established earlier would serve as useful tools to assess the phenotypic outcome of a knockdown in *FAM135B* in the WT sMNs. *FAM135B* knockdown was induced via a lentiviral based shRNA system in the WT sMNs as early as day 16 where post-mitotic sMNs were generated in culture. A high

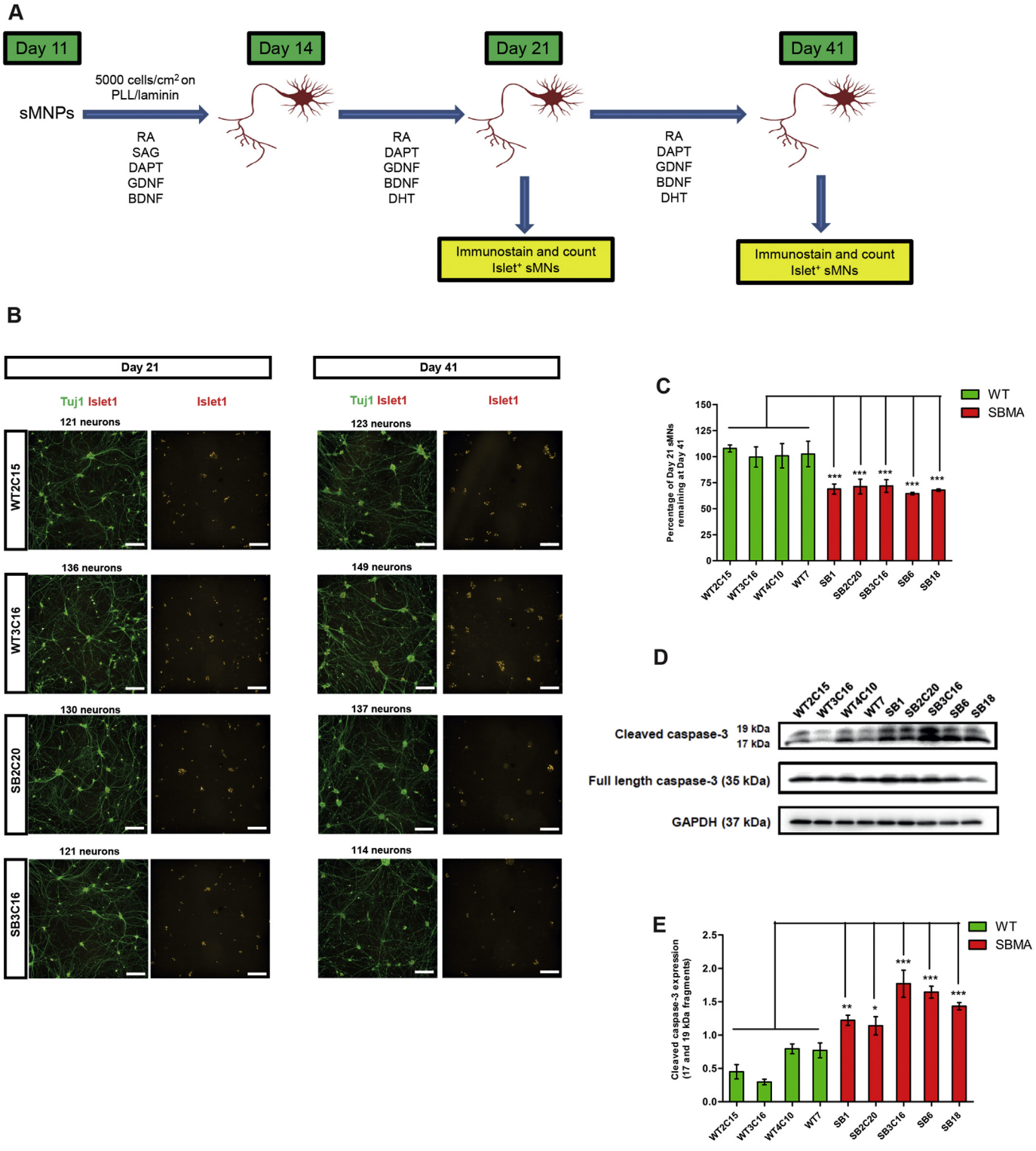

Fig. 3. Reduced survival of SBMA sMNs in prolonged culture.
(A) Schematic representation of sMN survival assay.
(B) Representative images of two WT and two SBMA sibling-matched sMN cultures stained for TUJ1 and ISLET1 at day 21 and 41. In the SBMA cultures, there were fewer ISLET1$^+$ sMNs at day 41 than at day 21 but not in the WT cultures. Scale bar, 200 μm.
(C) Quantification of day 21 ISLET1$^+$ sMNs remaining at day 41. Data represent mean ± SEM ($n = 3$), where n refers to the number of independent rounds of sMN differentiation. Comparisons are done by one-way ANOVA followed by Dunnett's test. ***$p < .001$. See also Fig. S3B.
(D) Representative western blot image showing levels of cleaved caspase-3 in WT and SBMA sMNs at day 41.
(E) Densitometric quantification of western blot image in (D). Values normalized to housekeeping gene GAPDH. Data represent mean ± SD (n = 3), where n refers to the number of independent rounds of sMN differentiation. Comparisons are done by one-way ANOVA followed by Dunnett's test. *$p < .05$, **$p < .01$, ***p < .001.

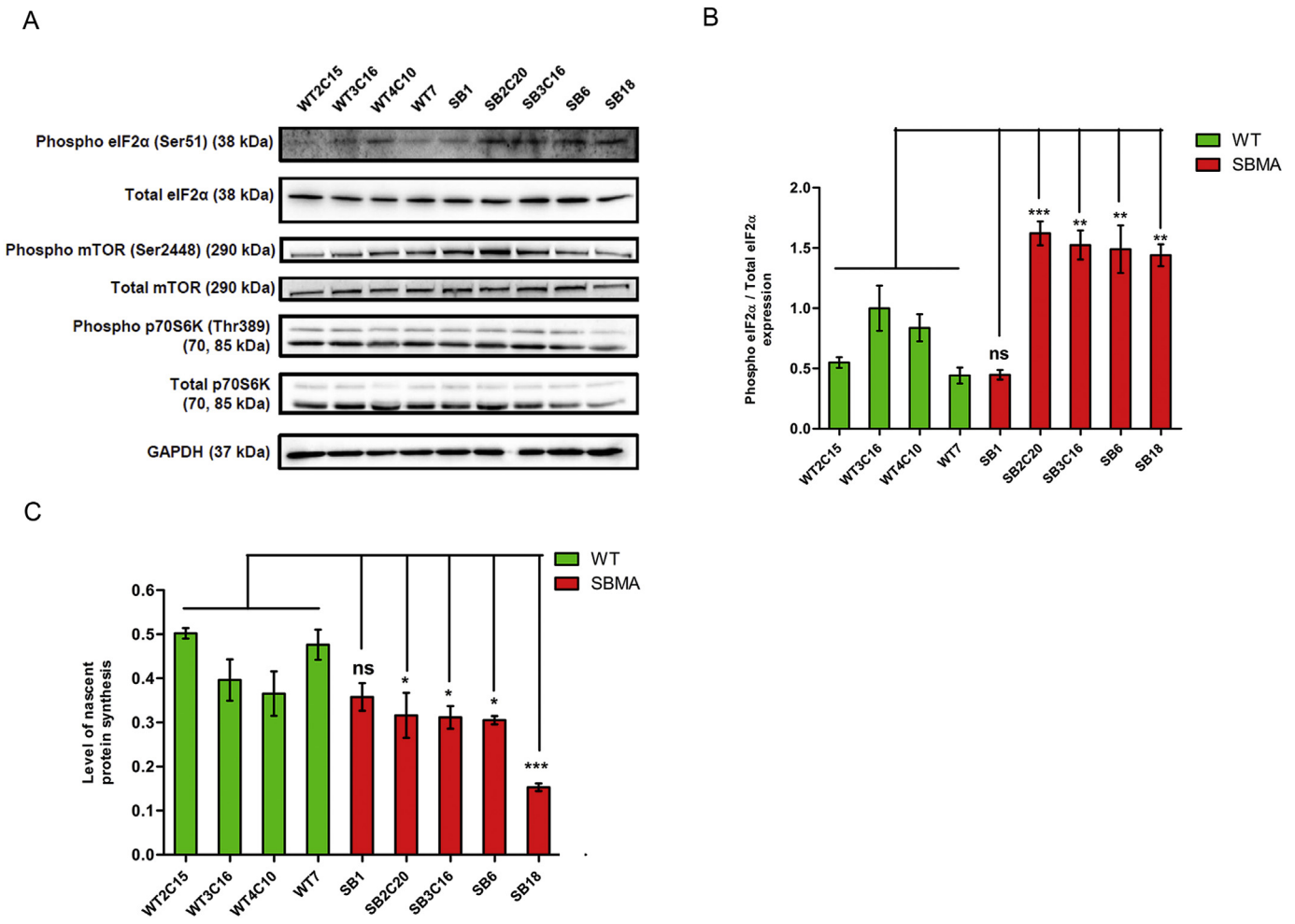

Fig. 4. Reduced protein translation in SBMA sMNs.
(A) Representative western blot showing levels of phosphorylated and total eIF2α in WT and SBMA sMNs at day 21.
(B) Densitometric quantification of western blot image in (C). Values are normalized to housekeeping gene GAPDH and total eIF2α. Data represent mean ± SD (n = 3), where n refers to the number of independent round of sMN differentiation. Comparisons are done by one-way ANOVA followed by Dunnett's test. ns- non-significant, **p < .01 and ***p < .001.
(C) Measurement of relative nascent protein synthesis using Click-iT® assay. Data represent mean ± SD (n = 3), where n refers to the number of independent rounds of sMN differentiation. Comparisons are done by one-way ANOVA followed by Dunnett's test. ns- non-significant, *p < .05, ***p < .001.

transduction efficiency of 60–70% was attained at day 21 through day 41 (Fig. 6B) with *FAM135B* gene expression levels being reduced by at least 50–60% throughout the entire duration of the assays in the WT sMN lines (Fig. 6C).

For the neurite length assay, the WT *FAM135B* knockdown sMN lines manifested a phenotype similar to the SBMA sMN lines where they showed less extensive neurite connections following prolonged culture from D21 through day 31 when compared to their WT sMN counterparts transduced with the non-silencing scrambled control shRNA (Fig. S5A). Quantification of the neurite length revealed that all four WT *FAM135B* knockdown sMN lines showed a significant reduction in average neurite length from day 21 through day 31 compared to their WT scrambled control sMN lines (Fig. 6D).

The effect of *FAM135B* knockdown on the survival of the sMNs was also assessed. For the sMN survival assay, the WT *FAM135B* knockdown sMN lines manifested a phenotype similar to the SBMA sMN lines as depicted by a reduction in the number of ISLET1+ sMNs at day 41 compared to day 21 (Fig. S5B). Quantification of the ISLET1+ sMNs at each time point revealed that all the four WT *FAM135B* knockdown sMN lines showed significantly lower sMN survival from day 21 through day 41 compared to their WT scrambled control counterparts (Fig. 6E).

Taken together, the reduction in sMN neurite length and survival upon *FAM135B* knockdown in the WT sMNs indicate that *FAM135B* plays a role in supporting sMN growth and survival, and implicates this previously uncharacterized gene as a player in SBMA disease pathology.

3. Discussion

iPSCs have been used to model neurodegenerative diseases in recent years. To model SBMA, we established two WT and three SBMA iPSC lines including two sibling-matched pairs (Narayanan et al., 2017). Together with these iPSC lines, we differentiated a total of four WT and five SBMA lines into sMNs for this current study. A key strength of our SBMA model is the generation of sMNs at high efficiency (~ 81.2%), higher than previously reported SBMA studies (Grunseich et al., 2014; Nihei et al., 2013). High efficiency sMN generation is crucial as it minimizes contribution of other cell types to the disease phenotypes observed. WT and SBMA iPSC lines generated sMNs with similar efficiencies indicating that the disease status of the cells did not alter the differentiation capacity of the iPSCs.

Phenotypic characterization of the WT and SBMA sMNs enabled us to observe disease-specific phenotypes in the SBMA sMNs. Firstly, the SBMA sMNs exhibited defects in neurite length compared to WT sMNs.

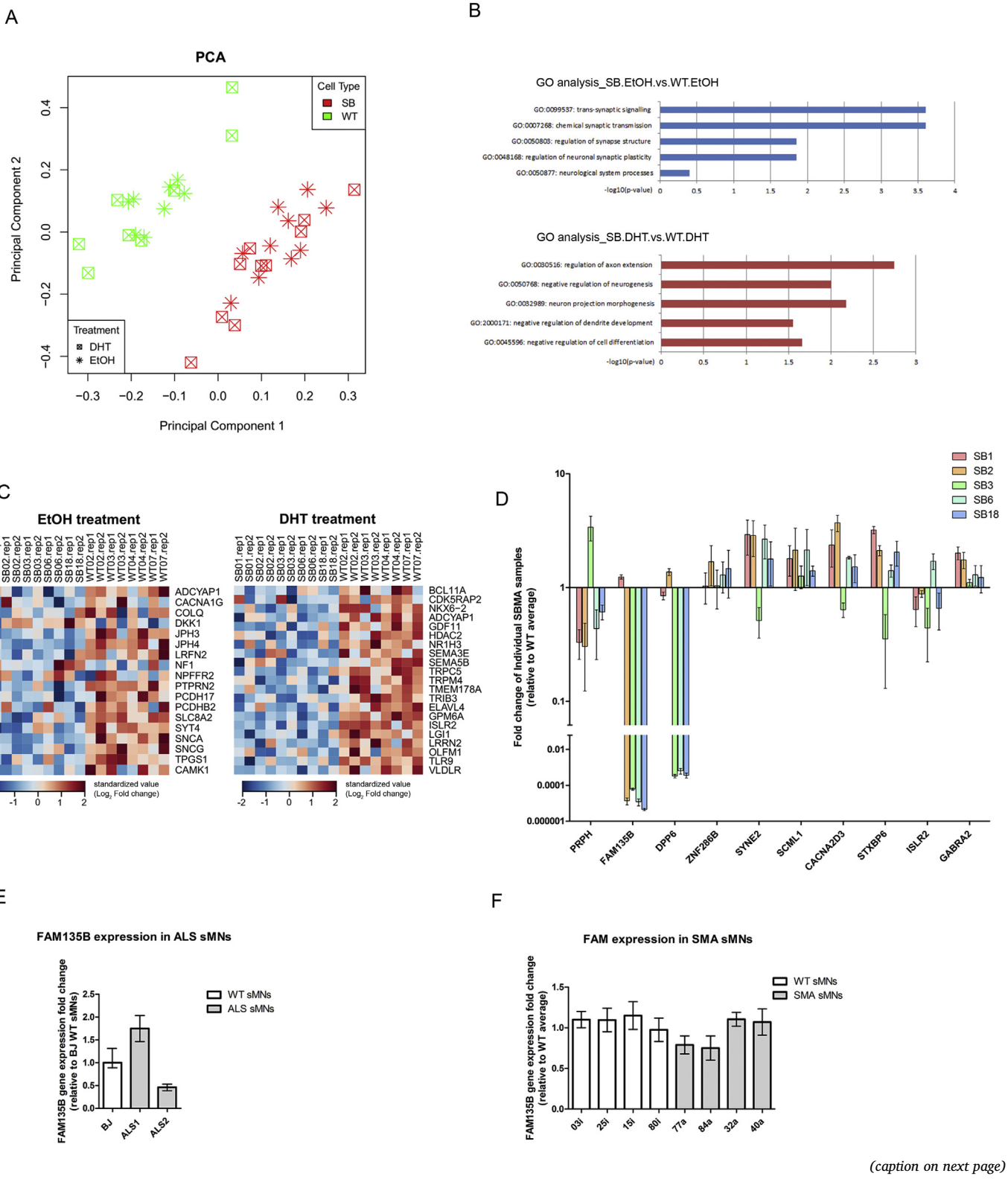

(caption on next page)

From the in vivo perspective, shortened neurite length could result in reduced synapse formation and synaptic transmission at the neuromuscular junction. Secondly, SBMA sMNs showed increased neurite blebbing compared to WT sMNs. Bleb-like features have also been observed in other neurodegenerative diseases such as dopaminergic neurons derived from Parkinson's iPSCs (Lin et al., 2016) and brain sections from Huntington's disease patients (Sapp et al., 1997). Increased neurite blebbing is indicative of poor neuron health and blebs are often described as features of apoptotic cells (Coleman et al., 2001). In our study, the neurite blebs occurred as early as day 21 and could be the first sign of degeneration before apoptosis of sMNs. Thirdly, our SBMA sMNs had lower survival than WT sMNs in prolonged culture. This is similar to observations in post-mortem spinal cord sections of SBMA patients where extensive depletion of lower motor neurons in the anterior horn of all spinal segments and brainstem motor nuclei was detected (Sobue et al., 1989). The sMNs from our SBMA model

Fig. 5. Gene expression profiling of SBMA and WT sMNs through microarray analysis.
(A) Principal component analysis (PCA) illustrating clustering of samples based on known covariates of either cell type (SBMA and WT) or treatment type (EtOH and DHT).
(B) Gene ontology (GO) analysis of downregulated genes in the SBMA sMNs compared to the WT sMNs at either the basal (EtOH) state or following DHT treatment.
(C) Heatmap of representative differentially expressed genes within the GO terms presented in Fig. 4B.
(D) qPCR validation of top 10 differentially expressed genes in the SB.DHT vs.WT.DHT gene list from microarray analysis. Results are normalized to housekeeping gene HPRT1 and presented as fold change differences in individual SBMA sMN lines relative to the average of WT sMN lines. Data represent mean ± SEM (n = 3), where n refers to three technical replicates included in the experiment. See also Fig. S4.
(E) qPCR analysis of *FAM135B* gene expression in ALS iPSC-derived sMN lines relative to WT iPSC-derived sMN line. Results are normalized to housekeeping gene HPRT1. Data represent mean ± SEM (n = 3), where n refers to three technical replicates included in the experiment. BJ, WT iPSC-derived sMN line; ALS1 and ALS2, SOD1 mutation and TDP mutation-associated ALS iPSC- derived sMN lines respectively.
(F) qPCR analysis of *FAM135B* gene expression in SMA iPSC-derived sMN lines relative to the average of WT iPSC-derived sMN lines. Results are normalized to housekeeping gene HPRT1. Data represent mean ± SEM (n = 3), where n refers to three technical replicates included in the experiment. 03i, 25i, 15i and 80i, WT iPSC-derived sMN lines; 77a, 84a, 32a and 40a, SMA iPSC-derived sMN lines with SMN1 gene-associated mutation resulting in low SMN1 gene copy number.

recapitulated the loss of sMNs observed in SBMA patients. This is in contrast with previously reported SBMA iPSC and mouse models where motor neuron numbers were preserved (Grunseich et al., 2014; Katsuno et al., 2002).

Molecular characterization revealed that the SBMA sMNs had lower AR expression compared to the WT sMNs. This is consistent with observations in SBMA patients where reduced AR levels may explain androgen insensitivity and reduced fertility in these patients (Warner et al., 1992). Reduced AR levels have also been observed in MN-1 cells overexpressing mutant AR (Lieberman et al., 2002). The reduced AR level could be attributed to the mutant AR having a shorter half-life and to a phenomenon called transcriptional interference, common in trinucleotide repeat disorders (Choong et al., 1996).

Protein translation is disrupted in our SBMA sMNs, possibly through modifications in the eIF2α signalling pathway. This can be viewed as a classical response to cellular stress in the SBMA sMNs to conserve metabolic energy for the repair of stress-induced damage elicited by the mutant AR. Additionally, previous studies have demonstrated the role of eIF2α phosphorylation and the subsequent halt in protein synthesis to reduced neurite formation, extension and synaptogenesis (Bellato and Hajj, 2016). Hence, besides being viewed as a response to cellular stress, eIF2α phosphorylation and the consequential impairment in protein synthesis could be viewed as deleterious processes causative of the neurodegenerative phenotypes observed in our SBMA model.

The severity of neurodegenerative phenotypes depicted in our study did not appear to correlate with CAG repeat length. There are indeed conflicting views on a direct link between disease severity and CAG repeat length (Atsuta et al., 2006; La Spada et al., 1991). Our study amongst others suggests that there are other unidentified modifiers of the disease outcome in SBMA including that of differences in genetic makeup of individuals which lend a unique twist to disease progression rate (Lund et al., 2001).

To better understand the effect of ligand binding on disease outcome, we performed experiments in the absence and presence of DHT, an AR agonist. Interestingly, the addition of DHT in our model system did not exacerbate the disease phenotypes. Furthermore, our microarray analysis revealed that biological pathways related to neuronal signalling were dysregulated both in the presence and absence of DHT and that ligand addition did not bring about drastic changes in the top genes implicated in the SBMA sMNs. Our observation that the disease phenotype was apparent at both the basal and DHT conditions is consistent with a study by Grunseich et al., 2014 where the disease phenotype of increased acetylated tubulin expression in polyQ-mutant AR expressing sMN lines, was detected in the presence and absence of DHT. In that study, it was suggested that the detection of nuclear AR at the basal state might have concealed any differences seen with DHT addition. In our study, we also recognise the possibility that progesterone present in the N2 supplement used in the culture media could be converted to DHT under basal conditions. 17β-HSD enzymes are known to be involved in the conversion of progesterone to DHT. By RT-PCR analysis, we found that all the WT and SBMA sMNs express the seven 17β-HSD enzymes under basal conditions (Fig. S6 and Table S7). This suggests that under basal conditions, the sMNs could convert progesterone in the culture media into DHT and this could explain why no exacerbation of the disease phenotypes were observed with further DHT addition.

Crucial insights into the SBMA disease mechanism were revealed by probing the transcriptome of sMNs in our SBMA model through microarray analysis. An intriguing finding is that a largely uncharacterized gene, *FAM135B*, was drastically downregulated in the SBMA sMNs compared to the WT sMNs. Interestingly, *FAM135B* was not downregulated in ALS and SMA sMNs, suggesting a specific role of *FAM135B* in SBMA rather than a generic role in motor neuron degeneration. Knockdown studies in WT sMNs revealed that reduction in *FAM135B* levels was sufficient to bring about a decrease in neurite length and sMN survival, likened to the phenotypes observed in the SBMA sMNs. Essentially, these observations shed light on the novel role of *FAM135B* in motor neuron growth and survival.

To date there have been no detailed studies that define a role of *FAM135B* in the nervous system. Nevertheless, insights into the properties of *FAM135B* allow us to hypothesize how its downregulation leads to neurodegeneration in SBMA. GO annotations related to *FAM135B* include "*hydrolase activity, acting on ester bonds*" and "*carboxyl ester hydrolase activity*" (GO:0052689) (Binns et al., 2009) thus broadly associating its molecular functions to a superfamily of genes coding for Carboxyesterases (EC 3.1.1.1) (Satoh and Hosokawa, 1998). The importance of carboxyesterases in the brain has been highlighted, wherein, its reduction has been linked to neurodegeneration. Ablation of the carboxyesterase *Neuropathy Target Esterase* (*NTE*) has been shown to result in vacuolation and subsequent loss of neurons (Akassoglou et al., 2004). Carboxyesterases including *Neuroligin*, *Neurotactin* and *Gliotactins* facilitate cell-cell adhesion in the CNS and aid in maintaining structural integrity of neurons (Fabrichny et al., 2007; Grisaru et al., 1999). These evidences depict the importance of carboxyesterases in the brain and with *FAM135B* sharing related GO annotations, its downregulation in the context of SBMA could have serious implications on neuronal growth and survival.

Yeast two-hybrid experiments have predicted KAT5 and *ZDHHC17* as interacting partners of *FAM135B* (Butland et al., 2014; Stelzl et al., 2005). *KAT5* codes for a histone acetyltransferase (HAT) involved in transcriptional activation of genes related to neuronal growth and survival (Oey et al., 2015; Pirooznia et al., 2012), DNA repair (Brochier and Langley, 2013) and axonal transport (Johnson et al., 2013). *ZDHHC17* codes for a palmitoyl transferase (PMT) involved in addition of amphipathic palmitoyl groups to neuronal proteins so that they can be targeted to the plasma membrane of neurons for the elicitation of vital biological functions related to neuronal signalling and communication (Huang et al., 2004). The catalytic activities of *KAT5* and *ZDHHC17* have been shown to be largely controlled by its binding partners (Huang et al., 2011; Jha et al., 2008). In the context of SBMA where its predicted interactor *FAM135B* is downregulated, it could be postulated that this may lead towards altered *KAT5* and *ZDHHC17*

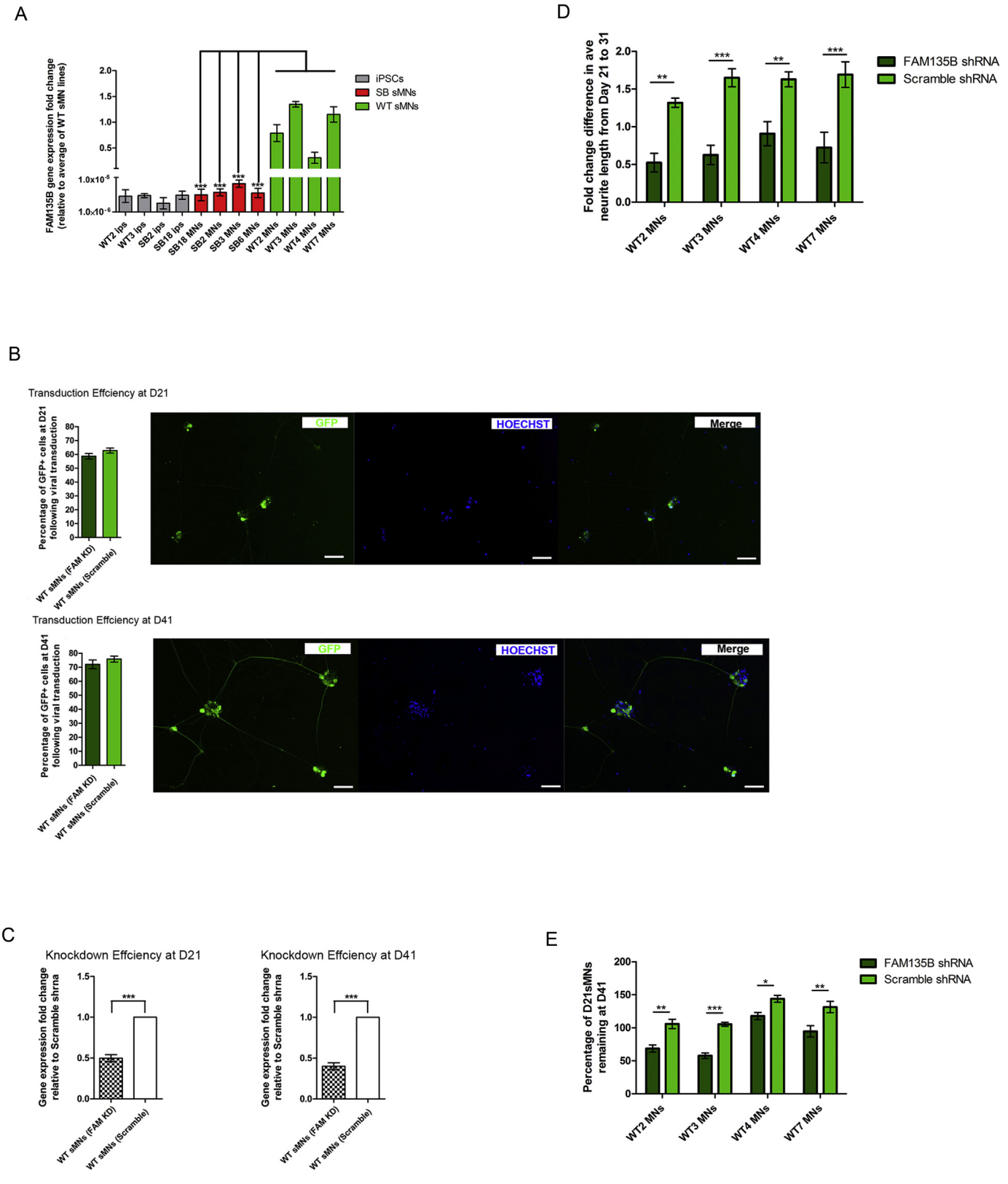

(caption on next page)

activities resulting in the elicitation of deleterious effects on neuronal function and survival. To add substantial basis to this hypothesis, a subset of *KAT5* gene targets like *CDK5RAP2* and *ZDHHC17* related targets including *ZNF286B, SYNE2, ISLR2*, *BRWD1, ZNF439, GPM6A,* and *STAMBPL1* were amongst the top 30 genes to be found dysregulated in the SBMA sMNs at both the EtOH and DHT conditions (Table S3). Taken together, these two interacting partners link *FAM135B* to diverse biological processes and neuronal signalling pathways. Further validation of these interacting partners of *FAM135B* and that of others, would provide key insights into the molecular link

Fig. 6. Investigating the functional role of *FAM135B* in SBMA.
(A) qPCR validation of *FAM135B* gene expression in individual WT and SBMA lines at the day 21 sMN or iPSC stage. Results are normalized to housekeeping gene HPRT1 and represented as fold change differences relative to the average of WT sMN lines. Data represent mean ± SEM (n = 3), where n refers to three technical replicates included in the experiment. Comparisons are done by one-way ANOVA followed by Dunnett's test. ***p < .001.
(B) (Right panels) Representative immunofluorescence images illustrating the efficiency of *FAM135B* and scrambled shRNA transduction at day 21 and day 41 in the WT sMN lines. sMNs were immunostained for anti-Turbo GFP antibody. Scale bar, 50 μm. (Left panels) Bar graph illustrating the average transduction efficiency of *FAM135B* and scrambled control shRNA at day 21 and day 41 for all four WT sMN lines, expressed as the number of Turbo-GFP$^+$ cells as a percentage of the number of Hoechst$^+$ cells. Data represent mean ± SD (n = 4), where n refers to the number of biological replicates.
(C) Bar graph illustrating the average knockdown efficiency of *FAM135B* shRNA at day 21 and 41 for all four WT sMN lines. Knockdown efficiency was determined by qRT-PCR analysis of *FAM135B* after *FAM135B* shRNA transduction. Results are presented as fold change differences in *FAM135B* gene expression relative to scrambled shRNA controls. Data represent mean ± SD (n = 4), where n refers to the number of biological replicates. Statistical significance was achieved using two-tailed unpaired *t*-test. ***p < .001.
(D) Quantification of average neurite length from day 21 through day 31 following *FAM135B* knockdown. Data represent mean ± SEM (n = 3), where n refers to the number of independent rounds of sMN differentiation. Comparisons are done by two-way ANOVA followed by Bonferroni's post-hoc test. **p < .01; ***p < .001. See also Fig. S5A.
(E) Quantification of percentage day 21 ISLET1$^+$ sMNs remaining at day 41 following *FAM135B* knockdown. Data represent mean ± SEM (n = 3), where n refers to the number of independent rounds of sMN differentiation. Comparisons are done by two-way ANOVA followed by Bonferroni's post-hoc test.*p < .05; **p < .01; ***p < .001. See also Fig. S5B.

between *FAM135B* and motor neuron degeneration in SBMA.

Future work could be focused on detailed investigation of the role of *FAM135B* in SBMA. With *FAM135B* proposed to play roles in neuronal survival, growth and maintenance of structural integrity, it could be speculated that an upregulation of which in SBMA sMNs could potentially result in a rescue of phenotype. As a proof of hypothesis, in WT sMNs where *FAM135B* is highly expressed, sMNs exhibited prolonged survival in culture, reduced apoptosis, and possessed long and structurally healthy neurites. Nevertheless, whether this is due to the sole upregulation of *FAM135B* is unclear. Furthermore, it would be useful to analyze if restoration of *FAM135B* in SBMA sMNs would bring about the regulated expression of key *KAT5* and *ZDHCC17* related gene targets, leading to improved neuronal survival and growth. In addition, investigating the relationship between polyQ AR and *FAM135B* would help delineate the role of *FAM135B* in SBMA. For instance, it would be useful to check if downregulation of AR in SBMA sMNs would lead to an upregulation of *FAM135B*, which would proof a direct link between presence of polyQ AR and *FAM135B*. Furthermore, investigating if *FAM135B* levels are downregulated in in vivo systems such as transgenic SBMA mice would help validate the in vitro findings. Conclusively, an in-depth exploration of the exact mechanism through which *FAM135B* mediates neurodegeneration in SBMA would aid in the development of effective therapies for this debilitating disease.

4. Experimental procedures

4.1. Differentiation of iPSCs to sMNs

Human iPSCs were differentiated to sMNs using a protocol described previously (Maury et al., 2015) with modifications. iPSCs were seeded on Matrigel-coated culture dishes in mTeSR1 medium. Two days later on day 0, MNP generation was initiated by culturing the iPSCs in N2B27 medium [Dulbecco's modified Eagle's medium/ Ham's F-12 medium (DMEM/F12):Neurobasal (Gibco) (1:1) supplemented with B27 (Gibco), N2 (Gibco), 0.5 μM ascorbic acid (Sigma), beta-mercaptoethanol (Gibco)] with 3 μM CHIR-99021 (Tocris), 40 μM SB-431542 (Tocris) and 0.2 μM LDN-193189 (Stemgent). On day 2, 100 nM retinoic acid (Sigma) and 500 nM SAG (Calbiochem) were added and on day 4, CHIR-99021, SB-431542 and LDN-193189 were removed. Subsequently, 10 μM DAPT (Tocris) was added on day 9. On day 11, the MNP colonies were dissociated using Accutase (Millipore) and seeded onto poly-L-lysine/laminin-coated dishes. They were then terminally differentiated to sMNs in N2B27 medium with 100 nM retinoic acid, 500 nM SAG, 10 μM DAPT, 10 ng/ml GDNF (Peprotech) and 20 ng/ml BDNF (Peprotech). For activation of AR, 50 nM DHT (Sigma) was added from day 14 onwards.

4.2. Immunofluorescence

Cells were fixed with 4% paraformaldehyde for 25 min at room temperature. The cells were then simultaneously blocked and permeabilized with 10% FBS and 0.01% Triton-X in PBS for one hour at room temperature. The cells were incubated at 4 °C overnight with primary antibodies at their appropriate concentration (Table S4). The next day, the cells were incubated with Alexa Fluor-conjugated secondary antibodies (Invitrogen) (1:1000 dilution) for one hour at room temperature in the dark and nuclei stained with Hoechst 33342 (Invitrogen). Images were acquired using Axio Observer.D1 inverted microscope (Zeiss) and analyzed using AxioVision software (Zeiss).

4.3. sMN survival and neurite assays

MNPs were terminally differentiated into sMNs on poly-L-lysine/laminin-coated 24-well culture dishes at 5000 cells/cm^2. From day 14 onwards, sMNs were treated with 50 nM DHT or ethanol (control). sMNs were fixed on day 21, 31 and 41 and immunostained for TUJ1 and ISLET1. Image acquisition was performed on Opera Phenix™ High Content Screening System (PerkinElmer) using Harmony® software (PerkinElmer) and images were analyzed using Columbus™ Image Data Storage and Analysis System.

For sMN survival analysis, the number of ISLET1$^+$ sMNs was counted at day 21 and 41 and normalized to the number of TUJ1$^+$ neurons at the respective timepoints. The number of ISLET1$^+$ sMNs at day 21 was then set as 100% and the number at day 41 was expressed as a percentage of day 21 to determine the percentage of day 21 sMNs remaining at day 41. For neurite length analysis, the total neurite length was measured at day 21 and day 31 using the CSIRO neurite detection module in Columbus™. For each timepoint, the total neurite length was normalized to the number of TUJ1$^+$ neurons to obtain the average neurite length. The average neurite length at day 31 was divided by that at day 21 to obtain the fold change increase. Neurite blebs were counted using the Spots detection module in Columbus™.

4.4. Measurement of nascent protein synthesis

Nascent protein synthesis was measured using the Click-iT® Plus OPP kit (Thermo Scientific), following manufacturer's instructions. Briefly, day 21 sMNs were incubated with 20 μM Click-iT® Plus OPP reagent for 30 min. Next, sMNs were incubated with Click-iT® Plus OPP reaction cocktail (containing Alexa Fluor® 594 picolyl azide) for 30 min. Nuclei were stained with HCS NuclearMask™ Blue Stain. Fluorescence intensity was measured using a microplate reader (Tecan). Alexa Fluor® 594 intensity from each well was normalized to the NuclearMask™ intensity from the same well to get the final value.

4.5. Microarray

500 ng of RNA was used to synthesize biotinylated cRNA using the TotalPrep RNA Amplification kit (Ambion). 750 ng of biotinylated cRNA was then hybridised onto the HumanHT-12 v4 Expression BeadChip (Illumina), according to the manufacturer's protocol. Microarray chips were then stained with streptavidin-Cy3 and hybridization fluorescence signals were detected by the Illumina BeadStation array reader. The microarray data was then imported into R and processed using R package “beadarray” (Dunning et al., 2007) and analyzed using R package “limma” (Smyth, 2005).

4.6. Statistical analysis

Statistical analysis was performed using GraphPad Prism software. Two-tailed Student's *t*-test was used for comparison of two groups. One-way or two-way ANOVA with post-hoc Dunnett's test or Bonferroni's test was used for comparison of more than two groups as stated in the figure legends. Data are presented as means ± SD or SEM and significance expressed as $*p < .05$, $**p < .01$, $***p < .001$.

Author contributions

M.S., G.N, J.C and L.W·S designed the study. M.S., G.N and L.W·S wrote the paper. M.S. and G.N performed all the experiments on iPSCs and sMNs and analyzed the data. M.S. and S.M analyzed the microarray data.

Acknowledgments

This research was funded by the Agency for Science, Technology and Research, Singapore. We thank Dr. Manfred Boehm (NHLBI, NIH) for gifting the iPSC line WT7 and Dr. Kenneth Fischbeck (NIH) for gifting the iPSC lines SB1, SB6 and SB18. We are grateful to Dr. Wang Jiaxu and Dr. Ng Shiyan for providing the SMA and ALS sMN samples respectively. We also thank Prof. Gavin Dawe, Prof. Mitchell Lai and Dr. Akshay Bhinge for helpful discussions and comments on this study. The authors declare no conflict of interest.

Appendix A. Supplementary data

Supplementary data to this article can be found online at https://doi.org/10.1016/j.nbd.2018.10.019.

References

Akassoglou, K., Malester, B., Xu, J., Tessarollo, L., Rosenbluth, J., Chao, M.V., 2004. Brain-specific deletion of neuropathy target esterase results in neurodegeneration. Proc. Natl. Acad. Sci. U. S. A. 101, 5075.

Atsuta, N., Watanabe, H., Ito, M., Banno, H., Suzuki, K., Katsuno, M., Tanaka, F., Tamakoshi, A., Sobue, G., 2006. Natural history of spinal and bulbar muscular atrophy (SBMA): a study of 223 Japanese patients. Brain 129, 1446–1455.

Beitel, L.K., Alvarado, C., Mokhtar, S., Paliouras, M., Trifiro, M., 2013. Mechanisms mediating spinal and bulbar muscular atrophy: investigations into polyglutamine-expanded androgen receptor function and dysfunction. Front. Neurol. 4, 53.

Bellato, H.M., Hajj, G.N., 2016. Translational control by eIF2alpha in neurons: beyond the stress response. Cytoskeleton (Hoboken, NJ) 73, 551–565.

Binns, D., Dimmer, E., Huntley, R., Barrell, D., O'Donovan, C., Apweiler, R., 2009. QuickGO: a web-based tool for Gene Ontology searching. Bioinformatics 25, 3045–3046.

Brochier, C., Langley, B., 2013. Chromatin modifications associated with DNA double-strand breaks repair as potential targets for neurological diseases. Neurotherapeutics 10, 817–830.

Butland, S.L., Sanders, S.S., Schmidt, M.E., Riechers, S.-P., Lin, D.T., Martin, D.D., Vaid, K., Graham, R.K., Singaraja, R.R., Wanker, E.E., 2014. The palmitoyl acyltransferase HIP14 shares a high proportion of interactors with huntingtin: implications for a role in the pathogenesis of Huntington's disease. Hum. Mol. Genet. 23, 4142–4160.

Chambers, S.M., Fasano, C.A., et al., 2009. Highly efficient neural conversion of human ES and iPS cells by dual inhibition of SMAD signaling. Nat. Biotechnol. 27 (3), 275–280.

Chevalier-Larsen, E.S., O'Brien, C.J., Wang, H., Jenkins, S.C., Holder, L., Lieberman, A.P., Merry, D.E., 2004. Castration restores function and neurofilament alterations of aged symptomatic males in a transgenic mouse model of spinal and bulbar muscular atrophy. J. Neurosci. 24, 4778–4786.

Choong, C.S., Kemppainen, J.A., Zhou, Z.X., Wilson, E.M., 1996. Reduced androgen receptor gene expression with first exon CAG repeat expansion. Mol. Endocrinol. 10, 1527–1535.

Coleman, M.L., Sahai, E.A., Yeo, M., Bosch, M., Dewar, A., Olson, M.F., 2001. Membrane blebbing during apoptosis results from caspase-mediated activation of ROCK I. Nat. Cell Biol. 3, 339.

Cortes, C.J., Miranda, H.C., Frankowski, H., Batlevi, Y., Young, J.E., Le, A., Ivanov, N., Sopher, B.L., Carromeu, C., Muotri, A.R., 2014. Polyglutamine-expanded androgen receptor interferes with TFEB to elicit autophagy defects in SBMA. Nat. Neurosci. 17, 1180.

Cruccu, G., Berardelli, A., Inghilleri, M., Manfredi, M., 1989. Functional organization of the trigeminal motor system in man: a neurophysiological study. Brain 112, 1333–1350.

Dunning, M.J., Smith, M.L., Ritchie, M.E., Tavaré, S., 2007. Beadarray: R classes and methods for Illumina bead-based data. Bioinformatics 23, 2183–2184.

Fabrichny, I.P., Leone, P., Sulzenbacher, G., Comoletti, D., Miller, M.T., Taylor, P., Bourne, Y., Marchot, P., 2007. Structural analysis of the synaptic protein neuroligin and its β-neurexin complex: determinants for folding and cell adhesion. Neuron 56, 979–991.

Grisaru, D., Sternfeld, M., Eldor, A., Glick, D., Soreq, H., 1999. Structural roles of acetylcholinesterase variants in biology and pathology. FEBS J. 264, 672–686.

Grunseich, C., Zukosky, K., Kats, I.R., Ghosh, L., Harmison, G.G., Bott, L.C., Rinaldi, C., Chen, K.-l., Chen, G., Boehm, M., 2014. Stem cell-derived motor neurons from spinal and bulbar muscular atrophy patients. Neurobiol. Dis. 70, 12–20.

Huang, K., Yanai, A., Kang, R., Arstikaitis, P., Singaraja, R.R., Metzler, M., Mullard, A., Haigh, B., Gauthier-Campbell, C., Gutekunst, C.-A., 2004. Huntingtin-interacting protein HIP14 is a palmitoyl transferase involved in palmitoylation and trafficking of multiple neuronal proteins. Neuron 44, 977–986.

Huang, K., Sanders, S.S., Kang, R., Carroll, J.B., Sutton, L., Wan, J., Singaraja, R., Young, F.B., Liu, L., El-Husseini, A., 2011. Wild-type HTT modulates the enzymatic activity of the neuronal palmitoyl transferase HIP14. Hum. Mol. Genet. 20, 3356–3365.

Hughes, D., Mallucci, G.R., 2018. The unfolded protein response in neurodegenerative disorders–therapeutic modulation of the PERK pathway. FEBS J. https://doi.org/10.1111/febs.14422.

Jha, S., Shibata, E., Dutta, A., 2008. Human Rvb1/Tip49 is required for the histone acetyltransferase activity of Tip60/NuA4 and for the downregulation of phosphorylation on H2AX after DNA damage. Mol. Cell. Biol. 28, 2690–2700.

Johnson, A.A., Sarthi, J., Pirooznia, S.K., Reube, W., Elefant, F., 2013. Increasing Tip60 HAT levels rescues axonal transport defects and associated behavioral phenotypes in a Drosophila Alzheimer's disease model. J. Neurosci. 33, 7535–7547.

Juarez-Hernandez, L., Polanco, M., Arosio, D., Basso, M., Pennuto, M., Musio, C., 2015. First electrophysiological study of neuron cell models of spinobulbar muscular atrophy SBMA. Eur. Biophys. J. Biophys. Lett. 44, S247 (Springer 233 SPRING ST, NEW YORK, NY 10013 USA).

Katsuno, M., Adachi, H., Kume, A., Li, M., Nakagomi, Y., Niwa, H., Sang, C., Kobayashi, Y., Doyu, M., Sobue, G., 2002. Testosterone reduction prevents phenotypic expression in a transgenic mouse model of spinal and bulbar muscular atrophy. Neuron 35, 843–854.

Katsuno, M., Adachi, H., Minamiyama, M., Waza, M., Tokui, K., Banno, H., Suzuki, K., Onoda, Y., Tanaka, F., Doyu, M., 2006. Reversible disruption of dynactin 1-mediated retrograde axonal transport in polyglutamine-induced motor neuron degeneration. J. Neurosci. 26, 12106–12117.

Katsuno, M., Banno, H., Suzuki, K., Adachi, H., Tanaka, F., Sobue, G., 2010. Clinical features and molecular mechanisms of spinal and bulbar muscular atrophy (SBMA). In: Diseases of DNA Repair. Springer, pp. 64–74.

La Spada, A.R., Wilson, E.M., Lubahn, D.B., Harding, A., Fischbeck, K.H., 1991. Androgen receptor gene mutations in X-linked spinal and bulbar muscular atrophy. Nature 352, 77.

Lieberman, A.P., Harmison, G., Strand, A.D., Olson, J.M., Fischbeck, K.H., 2002. Altered transcriptional regulation in cells expressing the expanded polyglutamine androgen receptor. Hum. Mol. Genet. 11, 1967–1976.

Lin, L., Göke, J., Cukuroglu, E., Dranias, M.R., Vandongen, A.M., Stanton, L.W., 2016. Molecular features underlying neurodegeneration identified through *in vitro* modeling of genetically diverse Parkinson's disease patients. Cell Rep. 15, 2411–2426.

Lund, A., Udd, B., Juvonen, V., Andersen, P.M., Cederquist, K., Davis, M., Gellera, C., Koèlmel, C., Ronnevi, L.-O., Sperfeld, A.-D., 2001. Multiple founder effects in spinal and bulbar muscular atrophy (SBMA, Kennedy disease) around the world. Eur. J. Hum. Genet. 9, 431.

Mandai, K., Guo, T., Hillaire, C.S., Meabon, J.S., Kanning, K.C., Bothwell, M., Ginty, D.D., 2009. LIG family receptor tyrosine kinase-associated proteins modulate growth factor signals during neural development. Neuron 63, 614–627.

Maury, Y., Côme, J., Piskorowski, R.A., Salah-Mohellibi, N., Chevaleyre, V., Peschanski, M., Martinat, C., Nedelec, S., 2015. Combinatorial analysis of developmental cues efficiently converts human pluripotent stem cells into multiple neuronal subtypes. Nat. Biotechnol. 33, 89.

Narayanan, G., Sheila, M., Chai, J., Stanton, L.W., 2017. Generation of sibling-matched induced pluripotent stem cell lines from spinal and bulbar muscular atrophy patients. Stem Cell Res. 20, 30–33.

Nihei, Y., Ito, D., Okada, Y., Akamatsu, W., Yagi, T., Yoshizaki, T., Okano, H., Suzuki, N., 2013. Enhanced aggregation of androgen receptor in induced pluripotent stem cell-derived neurons from spinal and bulbar muscular atrophy. J. Biol. Chem. 288, 8043–8052.

Oey, N.E., Leung, H.W., Ezhilarasan, R., Zhou, L., Beuerman, R.W., Vandongen, H.M.,

Vandongen, A.M., 2015. A neuronal activity-dependent dual function chromatin-modifying complex regulates arc expression. eNeuro *2*. ENEURO 2015 0020–0014.
Pirooznia, S.K., Chiu, K., Chan, M.T., Zimmerman, J.E., Elefant, F., 2012. Epigenetic regulation of axonal growth of Drosophila pacemaker cells by histone acetyltransferase tip60 controls sleep. Genetics 192, 1327–1345.
Ranganathan, S., Harmison, G.G., Meyertholen, K., Pennuto, M., Burnett, B.G., Fischbeck, K.H., 2008. Mitochondrial abnormalities in spinal and bulbar muscular atrophy. Hum. Mol. Genet. 18, 27–42.
Sapp, E., Schwarz, C., Chase, K., Bhide, P., Young, A., Penney, J., Vonsattel, J., Aronin, N., Difiglia, M., 1997. Huntingtin localization in brains of normal and Huntington's disease patients. Ann. Neurol. 42, 604–612.
Sareen, D., O'Rourke, J.G., Meera, P., Muhammad, A., Grant, S., Simpkinson, M., Bell, S., Carmona, S., Ornelas, L., Sahabian, A., 2013. Targeting RNA foci in iPSC-derived motor neurons from ALS patients with a C9ORF72 repeat expansion. Sci. Transl. Med. 5, 208ra149.
Satoh, T., Hosokawa, M., 1998. The mammalian carboxylesterases: from molecules to functions. Annu. Rev. Pharmacol. Toxicol. 38, 257–288.
Smyth, G.K., 2005. Limma: linear models for microarray data. In: Bioinformatics and Computational Biology Solutions Using R and Bioconductor. Springer, pp. 397–420.
Sobue, G., Hashizume, Y., Mukai, E., Hirayama, M., Mitsuma, T., Takahashi, A., 1989. X-linked recessive bulbospinal neuronopathy: a clinicopathological study. Brain 112, 209–232.
Stelzl, U., Worm, U., Lalowski, M., Haenig, C., Brembeck, F.H., Goehler, H., Stroedicke, M., Zenkner, M., Schoenherr, A., Koeppen, S., 2005. A human protein-protein interaction network: a resource for annotating the proteome. Cell 122, 957–968.
Sunkin, S.M., Ng, L., Lau, C., Dolbeare, T., Gilbert, T.L., Thompson, C.L., Hawrylycz, M., Dang, C., 2012. Allen Brain Atlas: an integrated spatio-temporal portal for exploring the central nervous system. Nucleic Acids Res. 41, D996–D1008.
Suzuki, K., Katsuno, M., Banno, H., Takeuchi, Y., Atsuta, N., Ito, M., Watanabe, H., Yamashita, F., Hori, N., Nakamura, T., 2007. CAG repeat size correlates to electrophysiological motor and sensory phenotypes in SBMA. Brain 131, 229–239.
Suzuki, E., Zhao, Y., Ito, S., Sawatsubashi, S., Murata, T., Furutani, T., Shirode, Y., Yamagata, K., Tanabe, M., Kimura, S., 2009. Aberrant E2F activation by polyglutamine expansion of androgen receptor in SBMA neurotoxicity. Proc. Natl. Acad. Sci. 106, 3818–3822.
Takeyama, K.-i., Ito, S., Yamamoto, A., Tanimoto, H., Furutani, T., Kanuka, H., Miura, M., Tabata, T., Kato, S., 2002. Androgen-dependent neurodegeneration by polyglutamine-expanded human androgen receptor in Drosophila. Neuron 35, 855–864.
Warner, C., Griffin, J., Wilson, J., Jacobs, L., Murray, K., Fischbeck, K., Dickoff, D., Griggs, R., 1992. X-linked spinomuscular atrophy A kindred with associated abnormal androgen receptor binding. Neurology 42, 2181.
Yu, Z., Dadgar, N., Albertelli, M., Scheller, A., Albin, R.L., Robins, D.M., Lieberman, A.P., 2006. Abnormalities of germ cell maturation and sertoli cell cytoskeleton in androgen receptor 113 CAG knock-in mice reveal toxic effects of the mutant protein. Am. J. Pathol. 168, 195–204.